Submitted for publication in Journal of Applied Physics

10-07-93

(2)

Atomic-Scale Friction and Microfriction of Graphite and Diamond Using Friction Force Microscopy

Ju-Ai Ruan and Bharat Bhushan

Computer Microtribology and Contamination Laboratory
The Ohio State University
206 West 18th Avenue
Columbus, Ohio 43210-1107

Abstract

Friction of graphite and diamond surfaces against a sharp silicon nitride tip was measured using a friction force microscope (FFM). *Atomic-scale friction* of a freshly cleaved highly oriented pyrolytic graphite (HOPG) exhibited the same periodicity as that of corresponding topography. However, the peaks in friction and those in corresponding topography profiles were displaced relative to each other. Using Fourier expansion of the interaction potential, we have calculated interatomic forces between the FFM tip and graphite surface. We have shown that the variations in atomic-scale friction and the observed displacement between the peaks in friction and those in corresponding topography can be explained by the variations in interatomic forces in the normal and lateral directions. At large scan sizes (50 nm x 50 nm or larger), the variation of friction for graphite and a single-crystal (IIa) diamond was found to follow the local slope of the sample surface, suggesting that a ratchet mechanism is operative in *microscale friction*.

I. INTRODUCTION

Understanding of adhesion, friction, wear, and lubrication of interfaces ("tribology") is crucial in optimizing the performance of machinery that require relative motion[1,2]. Many physical and chemical processes affect the tribological behavior of an interface in relative motion and makes the understanding of the underlying mechanisms difficult. The advent of new tools-atomic force microscope (AFM) (first developed by Binnig et al.[3] in 1986) and its modifications allow the study of contacts on a micro- to atomic scale. By modifying an AFM, Mate et al.[4] developed a friction force microscope (FFM) to measure atomic-scale friction of a sharp tungsten tip (with a radius of about 30 nm) in contact with a test surface, which is a convenient idealization of single asperity contact. The AFMs and FFMs have the necessary sensitivity to allow the application of forces weak enough ($\leq$ 1 nN) not to dislodge atoms from their sites during contact. Since the successful measurements of friction force by Mate et al.[4], several groups have combined measurements of normal and friction forces. These designs have used capacitance measurements[5], laser beam deflection[6,7] and optical interferometry[8]. Now, commercial instruments are available which allow the simultaneous measurements of surface topography and normal and friction forces.

In their pioneering study, Mate et al.[4] measured atomic-scale friction of a tungsten tip sliding on the basal plane of a single grain of highly oriented pyrolytic graphite (HOPG). Later the same group (Erlandsson et al.[9]) measured the atomic-scale friction between cleaved muscovite mica and a tungsten tip. For both graphite and mica, these authors reported that friction between a tungsten tip and the test sample surfaces exhibits the periodicity of the sample surface structure. They discussed atomic features in the friction force in terms of atomic-scale stick-slip. The magnitude of average friction force varied linearly with load with an atomic-scale coefficient of friction of 0.01 and 0.09 for graphite and mica, respectively. Germann et al.[10] measured the friction of a diamond tip on diamond (111) and (100) surfaces in ultrahigh vacuum (UHV). The friction force for (100) surface (with a step-like structure) exhibited periodic

features. They suggested that these features were associated with a 2x1 reconstructed surface convoluted over an asymmetric tip shape. The (111) surface showed features which could not be simply related to the surface structure. Hirano et al.[11] used mica instead of a sharp tip and measured the friction between a cylindrical and a flat single-crystal muscovite mica samples. They reported that frictional forces were anisotropic with respect to the lattice misfit angle between the two mica crystals. To date, a clear understanding of friction mechanism on a micro or nano scale does not exist.

Friction force images can also provide additional information which can be used to distinguish different chemical species in multicomponent organic films as shown by Overney et al.[12]. The same group (Meyer et al.[13, 14]) have also studied the lubrication behavior of Langmuir-Blodgett films using friction force microscope and observed a 10 fold reduction in friction for hydrocarbon covered surfaces compared to that of bare silicon substrates. (Also see O'Shea et al.[15]).

In this paper, we present data of simultaneous measurements of surface height and friction force profiles of graphite and diamond surfaces against a silicon nitride tip on micro- and atomic scales. The diamond surface did not show distinguishable atomic features, therefore atomic scale data are only reported for a graphite surface.

II. EXPERIMENTAL

We used an AFM/FFM from Digital Instruments (NanoScope III) for this study. The AFM/FFM used here (Fig. 1) can provide simultaneous measurements of friction force and surface topography. The sample is mounted on a piezoelectric tube (PZT) scanner which can precisely scan the sample in the horizontal (x-y) plane and can move the sample in the vertical (z) direction. A sharp tip at the free end of a Si_3N_4 beam is brought in contact with the sample. A laser beam from a laser diode is focused onto the back of the cantilever near its free end. The cantilever is

tilted downward at about 10 deg. with respect to the horizontal plane. The beam is reflected off the end of the cantilever and is directed through a mirror onto a split photodetector with four quadrants. Two quadrants [top (T) and bottom (B)] of the detector are used for measurement of the surface topography. As the sample is scanned under the tip, topographic features of the sample cause the tip to deflect in vertical direction. This tip deflection will change the direction of the reflected laser beam, changing the intensity difference between the top and bottom photodetector (AFM signal). A feedback circuit is used to modulate the voltage applied to the PZT scanner to adjust the height of the PZT, so that the cantilever vertical deflection or the normal force (given by the intensity difference between the top and bottom detector) will remain almost constant during scanning. Thus the PZT height variation is a direct measure of surface roughness of the sample.

Details of the friction measurement techniques have been described elsewhere[16]. We used the method in which the other two (L and R) quadrants of the photodetector (arranged horizontally) are used for the measurement of friction force being applied to the tip. The sample is scanned back and forth in a direction perpendicular to the longitudinal axis of the cantilever beam. Friction force between the sample and the tip produces a twisting of the cantilever. The laser beam is reflected out of the plane defined by the incident beam and the beam reflected from an untwisted cantilever. This produces an intensity difference of laser beam received between the left (L) and right (R) quadrants of the photodetector. This intensity difference (FFM signal) is directly related to the degree of twisting, hence to the magnitude of friction force. One problem associated with this method is that any misalignment between the laser beam and the photodetector axis would introduce error in the measurement. By adding the average of the two FFM signals obtained by scanning the sample in two opposite directions and dividing by two, and then subtracting this component from either profiles, the misalignment effect can be eliminated. Voltages corresponding to normal and friction forces can be converted to force units by following the force calibration procedures developed by Ruan and Bhushan[16]. By making measurements at various normal loads, average value of coefficient of friction is obtained which then can be used to convert the friction

profile to the coefficient of friction profile. Thus any directionality and local variation of friction can be easily measured. Surface topography data can be measured simultaneously with friction data and local relationship between the two profiles can be established. During AFM /FFM measurements, typical scanning speed was about 200 nm/s in the sliding direction and 2 nm/s in the direction perpendicular to the sliding. Microfriction measurements were made over 200 nm x 200 nm and 50 nm x 50 nm scan areas, whereas atomic scale friction were measured over 2 nm x 2 nm and 4 nm x 4 nm scan areas. The atomic scale images were magnified and only a 1 nm x 1 nm portion will be shown for clarity.

A highly oriented pyrolytic graphite (HOPG) [rms roughness (σ) = 0.3 nm over an 1 μm x 1 μm cleaved area] and a polished single-crystal natural diamond (IIa) (σ = 8.6 nm over an 1 μm x 1 μm area) were used in this study. Graphite was freshly cleaved for atomic scale measurement. After atomic scale measurements, the graphite surface was roughened (σ = 8.8 nm over an 1 μm x 1 μm area) using a sand paper (2400 mesh, 3-μm grit SiC). The sample was subsequently ultrasonically cleaned to remove debris from the surface. The roughened surface was used for microfriction measurements.

III. RESULTS AND DISCUSSION

A. Micro-Scale Friction

A gray-scale plot of the topography and corresponding micro-scale friction profiles of roughened graphite for a 200 nm x 200 nm scan size is shown in Fig. 2 (top and bottom, respectively). Also shown in this figure (middle) is the surface slope along the tip sliding direction (derivative of the surface topography) (Fig. 2b). Light color corresponds to high points in topography, slope, or friction and dark color corresponds to the corresponding low values. It is clear that the friction profile does not resemble the corresponding surface topography profile. However, the friction profile and the *slope* of the corresponding topography look remarkably

similar, which is true down to a 50 nm x 50 nm scan (Fig. 3). Similar trends are obtained for polished diamond, Fig. 4.

The resemblance between the slope of surface roughness profiles and the corresponding friction profiles can be explained by the ratchet mechanism initially proposed by Makinson[17] and later discussed by Tabor[18]. We consider a small tip sliding over an asperity making an angle θ with the horizontal plane, Fig. 6. The normal force (normal to the *general surface*) applied by the tip to the sample surface W is constant. Friction force F on the sample varies as a function of the surface roughness. It would be a constant $\mu_0 W$ for a uniform and smooth surface in the presence of "adhesive" friction mechanism. The force components along (S) and perpendicular to (N) *the local surface* of the sample (ascending part of the asperity) at the contact point are,

$$N = W\cos\theta + F\sin\theta \qquad \text{(A1)}$$

$$S = F\cos\theta - W\sin\theta \qquad \text{(A2)}$$

Since, when sliding occurs $S/N = \mu_0$ (coefficient of friction without roughness effect), we obtain the value of coefficient of friction including the roughness (ratchet) effects

$$\mu_1 = F/W = (\mu_0 + \tan\theta)/(1-\mu_0\tan\theta), \qquad \text{(A3a)}$$

where μ_1 is the local coefficient of friction. For a small $\mu_0\tan\theta$, Eq. (A3a) can be rewritten as

$$\mu_1 \sim \mu_0 + \tan\theta \qquad \text{(A3b)}$$

indicating that the asperity term is additive to the local coefficient of friction. Similarly, on the descending part of the asperity where $\tan\theta$ is negative,

$$\mu_2 \sim \mu_0 + \tan\theta$$

$$= \mu_0 - |\tan\theta| \qquad \text{(A4).}$$

For a symmetrical asperity, the average coefficient of friction the AFM tip experienced in traveling across the whole asperity is

$$\mu_{ave} = (\mu_1+\mu_2)/2$$

$$\sim\mu_0(1+\tan^2\theta) \qquad \text{(A5)}$$

if $\mu_0 \tan\theta$ is small. Therefore a symmetric asperity yields a contribution to coefficient of friction that is proportional to $\mu_0 \tan^2\theta$ averaged over the surface.

Other mechanism which also has a relationship between friction and surface shape is ploughing mechanism. According to Bowden and Tabor[1], the ploughing component of friction with tip sliding across an asperity is $\mu_p \sim \tan\theta$. Since in the FFM measurements, we notice little damage of the sample surface, the contribution by ploughing is expected to be negligible and the ratchet mechanism should be the dominant mechanism for the local variations in the friction profiles. With a tip sliding over the leading (ascending) edge of an asperity, the slope is positive, it is negative during sliding over the trailing (descending) edge of the asperity. Thus, friction is high at the leading edge of asperities and low at the trailing edge. The ratchet mechanism thus explain the correlation between slopes of the roughness profiles and friction profiles observed in Figs. 2 to 4. We note that in the ratchet mechanism, FFM tip is assumed to be small as compared to the size of asperities. This is valid since the typical radius of curvature of the tips is about 30 nm. The radius of curvature of the asperities of the samples measured here (the asperities that produce most of the friction variation) is found to be typically about 100-200 nm which is larger than that of the FFM tip.

B. Atomic-Scale Friction

The atomic-scale topography and friction profiles of freshly cleaved HOPG are shown in Fig. 5 (a). It is clearly seen that friction profile exhibits the periodicity of the graphite surface structure. However, the high points in the topography and the high friction points are shifted relative to each other. This can be seen more clearly in Fig. 5 (b). Atomic features could not be resolved for diamond and the corresponding friction data for diamond are not presented here.

We examine the atomic-scale variations of friction. Our primary purpose is to understand the spatial shift between peaks of friction and those of the corresponding topography. This shift

reflects the spatial displacement of maxima of normal force profile relative to those of frictional force profile for a given tip-sample distance. These forces can be calculated from the derivative of the interaction potential (energy) between atoms of the FFM tip and those of the sample surface. We will thus seek an analytical expression for this potential followed by expressions for the normal and lateral (friction) forces. Since our later discussion will deal with the topography of graphite, we first examine one of the relevant features of topographic images of graphite - "asymmetric atomic structure".

B.1. Asymmetric atomic structure and topographic images of Graphite

We first show in Fig. 7 the crystal structure of (0001) graphite surface which consists of multiple six-membered carbon rings ("benzene rings"). Each benzene ring consists of adjoining carbon atoms spaced 0.1415 nm apart (C-C distance). Each carbon atom has three neighbors arranged at the apices of an equilateral triangle. Three of the four valence electrons in each carbon atom are locked up with the tight covalent (sigma) bonds and the remaining valence electron is delocalized and free to wander over the surface. Thus adjacent layers have only secondary (van der Waals) attraction to each other. Adjacent layers [(0001) planes] are separated by 0.3354 nm and are staggered as shown in Fig. 7. Because of the staggering, only one-half of the carbon atoms have atoms directly above and below (A atoms) in the adjacent planes. The other half (B sites) atoms do not have atoms above or below; they fall above the center of the hexagon of the plane below. The H-sites (hollow sites) are in the center of the hexagon (do not have carbon atoms) in the top layer and have atoms directly below in the second plane (corresponding to B-sites in the second plane). The 7-atom hexagon connected by heavy broken lines in Fig. 7b (one atom is at the center of the hexagon) represents the location of B atoms (to be discussed later).

In few STM[19] (scanning tunneling microscopy) and AFM images[20], every atoms in the graphite surface have been observed. However in most STM[21-24] and AFM[25-27] measurements

of graphite, only every other carbon atoms on the surface were observed. The other carbon atoms were either not as prominent or "missing" completely. Thus the STM and AFM images consist of benzene rings having a distance between two nearest prominent atoms of about 0.246 nm with an additional carbon atom at the center of the ring (Fig. 7b). This loss of trigonal symmetry (between the A and B types of atoms) is what is called "asymmetric atomic structure" of graphite surface. In addition to the "asymmetric atomic structure", an enormous apparent height ("corrugation height") of atoms above the centers of the carbon rings (hollow points H, "holes") has also been reported. For example, for STM images, three hills and three saddle points were seen; a corrugation between hills and holes as high as 2.4 nm was observed[23, 28]. For AFM images, a corrugation distance of 0.02 nm between the holes and the highest sites (designated as B sites, to be discussed later) and 0.002 nm between the B sites and the second type of sites (designated as A sites) was observed[27].

A number of theoretical papers have appeared to explain the STM[19, 23-24, 28-33] and AFM[27,33-37] images of graphite and the associated phenomena. Tomanek et al.[24, 31] have calculated the electronic structure of graphite using *ab initio* pseudo potential local orbital method and concluded that the asymmetry is purely due to electronic effect. The Fermi surface of graphite collapses to a single point in the surface Brillouin zone, localized at A- and B- sites. The electronic states on A-sites are decoupled from those on B-sites. However, a coupling exists between A-site atoms in the adjacent plane and this coupling causes a dispersive band centered at E_F for electronic states located at A-sites. Whereas such a coupling does not exist between the B-site atoms on neighboring planes, leaving an undispersed state E_F at B-sites. The STM, which scans a narrow energy region below E_F detects all B-site states and only a very small fraction of A-site states. Therefore B-site atoms are more "visible" to STM than A-site atoms.

Batra and Ciraci[33] have performed self-consistent charge-density calculations, where surface relaxation was considered with three layers of graphite representing the (0001) surface.

They argued that since A-type atoms have neighbor atoms directly below, a weak interaction between them produces a weak chemical bond leading to a slight accumulation of charge between the planes of graphite under the A-sites. This accumulation may be at the expense of a slight depletion from the vacuum side of A-site atoms. The B-sites have no atoms below and hence have a slightly higher charge density in the vacuum region coming out of the B-sites compared to the A-sites. The charge density asymmetry between A-type and B-type atoms is even greatly amplified at Fermi energy E_F and the STM pattern might appear at times to show only B types of atoms which forms a centered hexagon of side 0.246 nm (Fig. 8). The H sites have the lowest charge density. Thus the highest corrugations should be between B and H sites. Batra and Ciraci[33] also predicted a corrugation values of about 0.1 nm based on their charge density calculation at Fermi surface.

For understanding of AFM images, interatomic forces present between the tip and the graphite surface need to be included. Batra and Ciraci[33] and Abraham and Batra[34] (also see Gould et al.[27]) calculated the interatomic forces using a self-consistent field method allowing for a full relaxation of the electronic charge distribution[33] or surface relaxation[34]. They found that if the tip is in close proximity with the sample (2.7 a.u., comparable to the first nearest neighbor distance in graphite), force at the B sites was highest followed by A sites then by H sites. (Forces at A and B sites are found to be quite similar in magnitude, however.) Batra and Ciraci[33] argued that the force difference between A and B sites may be due to the excess charge density at the B sites since the bands at E_F are centered on B atoms. At higher tip-sample spacing, the relative distribution of forces changes. At 4.7 a.u., the force at the H sites is higher than that at A and B sites. Thus, depending upon the tip proximity, different images can be observed. With a tip in close proximity with the samples, only B atoms may be more visible as seen in AFM images. It should be noted that Batra and Ciraci's[33] calculated force difference between A and B sites is very small, not significant enough for a firm distinction between the two types of atoms. In principle, both A type and B type atoms should be visible to the AFM tip[33].

Mizes et al.[19] and later Gould et al.[27] have offered another interpretation for the STM and AFM images of graphite, respectively. They have shown that the asymmetry and a variety experimental images could be reproduced by calculation if it can be assumed that there are two atoms at the end of the STM or AFM tip. Each tip-atom can image the surface and a relative phase shift between the two images "seen" by the individual tip-atom would produce a resultant (experimental) image, whose pattern can be different from the honeycomb structure of graphite lattice.

While these explanations for the graphite STM and AFM images seem to be convincing, they probably have not provided the complete picture. For example, as reported by Land et al.[38], the asymmetry (appearance of every other carbon atom) was observed in STM images even for single-layer graphite deposited on Pt. As pointed out by Land et al.[38], though electronic interaction between the graphite and the Pt substrate is strong, this does not allow a distinction between *two unique* types of carbon sites. Therefore the observed "asymmetric atomic structure" of graphite cannot be fully explained by Batra et al.'s[30,33] or Tomanek et al.'s[24, 31] theories. Mizes et al.'s[19] and Gould et al.'s[27] theories do not have the difficulty in explaining Land et al.'s[38] data. Yet it is not easy to verify their theories since the precise shape of the STM and AFM tips is unknown. As we shall see later, there may be other factors which could introduce the "asymmetry of the atomic structure" of graphite.

B.2. Friction force images of graphite

We now focus on the spatial shift between peaks of friction and those of the corresponding topography of graphite. As mentioned early, this shift reflects the spatial displacement of maxima of normal force relative to those of lateral force, and these forces can be calculated from the spatial derivative of the interaction potential (energy) between atoms of the FFM tip and those of the sample surface. For a precise analysis of the interaction force between the tip and sample surfaces, surface relaxation of both the sample and the tip as a result of their

mutual interaction must be included. An exact solution to this complicated interacting system has not been available and can hardly be obtained since, first of all, the precise shape of the tip (physical arrangement of the outer most atoms of the tip) is unknown. In most theoretical calculations the tip was treated as "rigid" or as a single-atom tip with no relaxation, only the graphite surface was allowed to relax[27-28, 30, 33-37]. With this and some additional approximations, calculations (such as the one using continuum elasticity theory with parameters obtained from first principles total-energy calculation within local-density approximation[35-37], self-consistent charge-density calculation[30, 33]) have provided some insight towards understanding the observed abnormalities in STM and AFM images of graphite, such as the observed huge corrugation height[23, 28]. While these calculations can be some what accurate depending on the specific problems they are dealing with, they are performed numerically and are time consuming particularly if tip relaxation is allowed.

Since our objective here is to understand the relative spatial shift between maxima in topography (or normal force) and those in friction, a simple *analytical expression* for the normal and lateral forces should be more instructive than numerical calculations. These forces will be calculated from the spatial derivative of the interaction potential between the tip and the sample. Approximations are necessary in deriving such an expression. The simplest approach is to use Fourier expansion to represent the interaction potential. Since the observed topographical features of graphite are dominated by low wave vector components, it is sufficient to keep only a few low wave vector terms in the Fourier expansion for the total interaction potential which leads to the desirable simplicity. We will make two assumptions: (1) the interaction potential between the tip and graphite surface (denoted as "total interaction potential") equals the sum of the interaction potential between individual tip atoms and carbon atoms of graphite (denoted as "partial potential"), and the tip atoms interact with carbon atoms of graphite through pair-wise potential which is same for all graphite atoms; (2) the pair-wise interaction potential between a

tip atom and a carbon atom can be approximated by Lennard-Jones potential. For simplicity, we will consider a single atom to represent the FFM tip.

The periodic structure of graphite surface (Fig. 9) warrants that the interaction potential between a tip atom and the graphite surface is also periodic with the same periodicity as that of the graphite surface plane, so that the total interaction potential $u(\mathbf{r})$ ($\mathbf{r}$ is the position of the tip with respect to the graphite surface) takes the form of

$$u(\mathbf{r}+\mathbf{l}) = u(\mathbf{r}) \tag{B1}$$

with

$$\mathbf{l}=l_1\mathbf{a}_1+l_2\mathbf{a}_2 \tag{B2}$$

where l_1 and l_2 are integers and $\mathbf{a}_1$ and $\mathbf{a}_2$ are the unit lattice vectors in the surface plane (Fig. 9). The periodic nature of the interaction potential [Eq. (B1)] allows $u(\mathbf{r})$ to be expressed in terms of the following Fourier expansion

$$u(\mathbf{r})=\sum_{g} w_g(z) \exp(i\mathbf{g}\cdot\boldsymbol{\tau}) \tag{B3}$$

where $\boldsymbol{\tau}$ is the two-dimensional translation vector [in the (0001) graphite surface plane], $z=|\mathbf{z}|$ and $\mathbf{z}$ is in the direction perpendicular to the graphite surface, $\mathbf{g}$ is the multiples of the reciprocal lattice vectors $\mathbf{b}_1$ and $\mathbf{b}_2$:

$$\mathbf{g}=2\pi(g_1\mathbf{b}_1 + g_2\mathbf{b}_2), \tag{B4}$$

where g_1 and g_2 are integers and $\mathbf{b}_1$ and $\mathbf{b}_2$ are defined by

$$\mathbf{a}_1.\mathbf{b}_1=1=\mathbf{a}_2.\mathbf{b}_2,$$

$$\mathbf{a}_1.\mathbf{b}_2=0=\mathbf{a}_2.\mathbf{b}_1.$$

$w_g(z)$ in equation (B3) is the Fourier coefficient of the plane wave with a wave vector $\mathbf{g}$. There is no periodicity in the direction (z) perpendicular to the sample surface plane.

Based on pair-wise additivity[39] (assumption 1), the total interaction potential $u(\mathbf{r})$ between the tip atom and the graphite crystal can be regarded as the sum of partial interaction

potentials (the interaction between the tip atom and *individual* carbon atoms of graphite)

$$u(\mathbf{r}) = \sum_{\alpha} \sum_{l1,l2} \sum_{k} u_{ts}(z_\alpha, \boldsymbol{\tau}+\mathbf{l}+\mathbf{m}_k) \qquad \text{(B5)}$$

where $u_{ts}(z_\alpha, \boldsymbol{\tau}+\mathbf{l}+\mathbf{m}_k)$ is the partial interaction potential between the tip atom and the carbon atom *in the* α*th* plane in the graphite crystal located at a vertical distance z_α from the tip atom, k indicates the kth atom in a unit cell and the position of the atom in the plane is given by $\mathbf{l}+\mathbf{m}_k$.

Equations (B3) and (B5) are different expressions of the same physical interaction. Thus $w_g(z)$ in Eq.(B3) can be calculated by calculating the two dimensional Fourier transformation of $u_{ts}(z_\alpha, \boldsymbol{\tau}+\mathbf{l}+\mathbf{m}_k)$ in equation (B5).

$$w_g(z) = \sum_{\alpha} w_g(z_\alpha) \qquad \text{(B6)}$$

with

$$w_g(z_\alpha) = \frac{1}{A} \sum_{l1,l2} \sum_{k} \int_{A} \exp(-i\mathbf{g}.\boldsymbol{\tau})\, u_{ts}(z_\alpha, \boldsymbol{\tau}+\mathbf{l}+\mathbf{m}_k)\, d\tau$$

$$= \frac{1}{A} \sum_{k} \exp(i\mathbf{g}.\mathbf{m}_k) \int_{0}^{\infty} \exp(-i\mathbf{g}.\mathbf{t})\, u_{ts}(z_\alpha, \mathbf{t})\, dt \qquad \text{(B7)}$$

where A is the smallest area representing the surface periodic structure[40] (defined in this paper as *"2-D primitive unit cell"*), and $\mathbf{t}=\boldsymbol{\tau}+\mathbf{l}+\mathbf{m}_k$. Equation (B6) means that the coefficient $w_g(z)$ of the Fourier component with wave vector $\mathbf{g}$ is the sum of $w_g(z_\alpha)$, the components from individual plane.

Detailed calculation of $w_g(z)$ requires a specific function for $u_{ts}(\mathbf{r})$. Steele[39] has calculated $w_g(z_\alpha)$ using the *Lennard-Jones potential*[40] (assumption 2) as the interaction potential between a gas atom (tip atom) and individual atoms in a solid $u_{ts}(r_i)$,

$$u_{ts}(r_i) = 4\varepsilon_{ts}\left\{\left(\frac{\sigma}{r_i}\right)^{12} - \left(\frac{\sigma}{r_i}\right)^{6}\right\} \qquad \text{(B8)}$$

where r_i is the distance between the tip atom and the *i*th atom in the solid. The parameter which is of important concern here is the value σ, which is typically between 0.2 to 0.4 nm[40]. Using this potential, Steele[39] found that

$$w_0(z_\alpha) = \varepsilon_{ts} \frac{2\pi}{A} q \left(\frac{2\sigma^{12}}{5 z_\alpha^{10}} - \frac{\sigma^6}{z_\alpha^4}\right) \tag{B9}$$

and

$$w_g(z_\alpha) = \varepsilon_{ts} \frac{2\pi}{A} \left[\frac{\sigma^{12}}{30}\left(\frac{g}{2z_\alpha}\right)^5 K_5(g z_\alpha) - 2\sigma^6 \left(\frac{g}{2z_\alpha}\right)^4 K_2(g z_\alpha)\right], \tag{B10}$$

where q is the total number of atoms per 2-D primitive unit cell (for graphite, q=2) and K_n is the modified Bessel function of the second kind. Steele[39] also mentioned that it is the atoms on the surface plane which make appreciable contribution to the interaction. This is because both $w_0(z_\alpha)$ and $w_g(z_\alpha)$ decrease rapidly with the increase of z_α. [Bassel function $K_n(x)$ goes as $(\pi/2x)^{1/2}\exp(-x)$, at large x.] By retaining only the first plane (surface plane) in the summation in Eq.(B6), and letting $z_\alpha = z$, we have

$$\begin{aligned} u(r) \sim & w_0(z) + \sum_{g>0} \sum_{k=1}^{q} w_g(z) \exp[i\mathbf{g}.(\mathbf{m}_k + \boldsymbol{\tau})] \\ = & C(z) + \sum_{g>0} \sum_{k=1}^{q} D(g, z) \exp[i\mathbf{g}.(\mathbf{m}_k + \boldsymbol{\tau})] \end{aligned} \tag{B11}$$

where g is the magnitude of $\mathbf{g}$, $g = |\mathbf{g}| = \frac{2\pi}{a}(g_1^2 + g_2^2 - g_1 g_2)^{1/2}$ and

$$C(z) = w_0(z_\alpha) = \varepsilon_{ts} \frac{2\pi}{A} q \left(\frac{2\sigma^{12}}{5 z_\alpha^{10}} - \frac{\sigma^6}{z_\alpha^4}\right), \tag{B12}$$

$$D(g, z) = w_g(z_\alpha) = \varepsilon_{ts} \frac{2\pi}{A} \left[\frac{\sigma^{12}}{30}\left(\frac{g}{2z_\alpha}\right)^5 K_5(g z_\alpha) - 2\sigma^6 \left(\frac{g}{2z_\alpha}\right)^4 K_2(g z_\alpha)\right]. \tag{B13}$$

There are two carbon atoms per 2-D primitive unit cell in graphite basal plane. If we choose $\boldsymbol{\tau}$=0 to be at a hollow point and the 2-D primitive unit cell is chosen as shown in Fig. 9, then $\mathbf{m}_k$ for the two atoms in the 2-D unit cell indicated in Fig. 9 are located at (1/3, 1/3)*a*, (2/3,

2/3)a (a is the lattice constant of the 2-D unit cell representing the distance between the centers of nearest hexagons). Summation over $\mathbf{m}_k$ gives a value of $2\cos[\frac{2\pi}{3}(g_1 + g_2)]$. Therefore

$$u(r) = C(z) + 2\sum_{g>0} D(g,z)\exp(i\mathbf{g}\cdot\boldsymbol{\tau})\cos[\frac{2\pi}{3}(g_1 + g_2)] \quad \text{(B14)}$$

As mentioned early, it is only the small wave vector components that give the major contribution to the interaction potential because D(g, z) in Eq. (13) decrease rapidly with the increase of g. To the first order, we consider only the first six wave vectors, for which $|g| = 2\pi/a$ and $\cos[2\pi/3(g_1+g_2)] = -1/2$. With x and y coordinates chosen as shown in Fig. 9, $\boldsymbol{\tau} = x+y$ can be expressed in terms of $\mathbf{a}_1$ and $\mathbf{a}_2$ with

$$\mathbf{x} = \frac{x}{a}(\mathbf{a}_1 - \mathbf{a}_2),$$

$$\mathbf{y} = \frac{y}{\sqrt{3}}(\mathbf{a}_1 + \mathbf{a}_2).$$

We have

$$u(r) = C(z) - D(2\pi/a, z)\,[2\cos(\frac{2\pi y}{a\sqrt{3}})\cos(\frac{2\pi x}{a}) + \cos(\frac{4\pi y}{a\sqrt{3}})]. \quad \text{(B15)}$$

Normal and lateral forces at any point can be calculated using $\mathbf{F} = -\nabla u(r)$. We obtain

$$F_x = -D(2\pi/a, z)\frac{2\pi}{a}\,[2\cos(\frac{2\pi y}{a\sqrt{3}})\sin(\frac{2\pi x}{a})]; \quad \text{(B16)}$$

$$F_y = -D(2\pi/a, z)\frac{4\pi}{\sqrt{3}a}\,[\sin(\frac{2\pi y}{a\sqrt{3}})\cos(\frac{2\pi x}{a}) + \sin(\frac{4\pi y}{a\sqrt{3}})]; \quad \text{(B17)}$$

$$F_z = -\frac{dC(z)}{dz} + \frac{dD(2\pi/a, z)}{dz}\,[2\cos(\frac{2\pi y}{a\sqrt{3}})\cos(\frac{2\pi x}{a}) + \cos(\frac{4\pi y}{a\sqrt{3}})]. \quad \text{(B18)}$$

As expected, the force components are periodic with a periodicity a in the x direction and $\sqrt{3}a$ in the y direction as shown in Fig. 9. There are at least one minimum and one maximum for each force component within each 2-D primitive unit cell. The location (x_0, y_0) of the extremes of each of the force components satisfies the conditions that[41]

$$\frac{\partial Fi}{\partial x} = 0, \quad \frac{\partial Fi}{\partial y} = 0, \quad \text{and} \quad \begin{vmatrix} \frac{\partial^2 Fi}{\partial x \partial y} & \frac{\partial^2 Fi}{\partial x^2} \\ \frac{\partial^2 Fi}{\partial y^2} & \frac{\partial^2 Fi}{\partial x \partial y} \end{vmatrix} < 0,$$

where i=x, y, or z. If at (x_0, y_0) $\frac{\partial^2 F_i}{\partial x^2} < 0$ and $\frac{\partial^2 F_i}{\partial y^2} < 0$, then F_i has a maximum at this point. Similarly, F_i has a minimum if $\frac{\partial^2 F_i}{\partial x^2} > 0$ and $\frac{\partial^2 F_i}{\partial y^2} > 0$ at (x_0, y_0).

The extremes of normal and lateral forces were calculated for the z range where $\frac{dD(2\pi/a,z)}{dz} < 0$ and $D(2\pi/a, z) > 0$. (In the region where $\frac{dD(2\pi/a,z)}{dz} > 0$ or $D(2\pi/a, z) < 0$, the maxima and minima of corresponding force components will flop their positions.) For the normal force (F_z), the minimum is at (x=0, y=0) and the maxima are at (x=0, $y=\frac{a}{\sqrt{3}}$) and (x=0, $y=\frac{2a}{\sqrt{3}}$) within the 2-D primitive unit cell indicated in Fig. 9. The positions of the maxima are precisely where the carbon atoms are located at and the position of minimum is at a "hollow point". The position in between the two maxima at (x=0, $y=\frac{\sqrt{3}}{2}a$) is also a special point. It is easy to see that if the x coordinate is set at x=0, then F_z has a minimum at $y=\frac{\sqrt{3}}{2}a$ when the y coordinate is varied. On the other hand, at $y=\frac{\sqrt{3}}{2}a$, F_z has a maximum at x=0 when the x coordinate is varied. Therefore the point at (x=0, $y=\frac{\sqrt{3}}{2}a$) is a saddle point. Normal force F_z at the saddle point is only slightly smaller (by 10%) than that at the two maxima. The extremes of the lateral forces (F_x and F_y) were calculated and are summarized in Table 1 and Fig. 9. The extremes of F_x along the x axis and F_y along the y axis are also shown in Fig. 9, together with detailed variation of force components along these two axes. We note that there is a relative shift between maxima of lateral force and those of normal force. The shift for both F_x and F_y is in the manner that the lateral force is to push the FFM tip atom away from the points where the interaction potential is the largest.

Examining the experimental data presented in Fig. 5 for the normal force, we note that only one maximum was observed per 2-D primitive unit cell, i.e., only every other atoms were observed. On the other hand, calculation (within the first order approximation) indicates two

maxima for normal force, with a saddle point which is 10% smaller than the maxima in between two nearest maxima. (By extending the calculation to second order, we found that the difference between maxima and saddle points is even smaller.) The calculation result is expected since we use a single atom to represent the tip and only the top (surface) layer of graphite was retained in our approximation. By including more layers in the calculation, modification to the normal force is expected to be small since the force decrease rapidly with the increase of the distance between the tip atom and the underlying layers. This is consistent with Abraham and Batra's[34] calculation [where six (0001) layers were considered]. They found that the (monoatomic) tip experiences very similar forces when it is placed above an A or B site. Consequently, by considering only the normal force between the tip and the graphite surface, a monoatomic tip would detect *every atom* of the surface and the image would give a *honeycomb structure*.

The discrepancy between the calculated and the experimental (AFM/FFM) data for the number of maxima in normal force profile can be reconciled by assuming that there are two atoms at the end of the AFM tip using Mizes et al.'s[19] and Gould et al.'s[27] explanation discussed previously, or assuming that there is a graphite flake at the end of the FFM tip. However, the correctness of this assumption remains to be verified since the exact shape of the tip is unknown. We note that in all reported theoretical calculations of topographic imaging of graphite, normal force is the only force that has been considered. This is valid if the tip-atoms are truly "rigidly" fixed to the tip substrate. However, there is no reason to believe that this must be the case. Intuitively, if a sample surface (such as graphite) is allowed to deform under the interaction force between the tip and the sample, the tip surface can be deformed as well. In the case of a single-atom at the end of a tip, this atom may relax laterally due to a lateral force acting from the sample. It is conceivable that the atom at the end of the AFM/FFM tip can actually hop around[42] under the influence of lateral (friction) force. For example, considering an FFM tip with a single atom at its end moving across a graphite surface in y direction as shown in Fig. 9, the tip atom experiences a lateral force towards $-y$ direction before it encounters the first carbon atom of the

indicated 2-D primitive unit cell. Lateral force is zero at the middle of these two carbon atoms. After the tip crosses the second carbon atom of this 2-D unit cell, lateral force acting on the tip-atom is strong and acts towards y direction. The tip atom may relax from one position to another due to the variation of lateral force. During the relaxation the normal force on the tip will increase/decrease slightly which will be compensated by the sample movement (the sample will be lowered/raised to maintain the normal force almost constant). Therefore it may appear that the "real" maximum of normal force as seen by the tip atom is located close to one of these two carbon atoms.

Based on the analysis presented in this section, one may predict the relative shift between maxima of normal force and those of friction force observed in Fig. 5. If we assume that the FFM tip is approximately sliding in ($\hat{\mathbf{x}}$-0.16$\hat{\mathbf{y}}$) direction ($\hat{\mathbf{x}}$ and $\hat{\mathbf{y}}$ are unit vectors along x and y axes, respectively), and that the normal force maxima occur at the location of the second carbon atom in the indicated 2-D primitive unit cell and its equivalent locations, we then determine a spatial displacement between maxima of topography and those of friction as shown in Fig. 10. This figure looks similar to Fig. 5b from the experiment. It should be pointed out that this is a simplified analysis involving certain assumptions. More detailed calculation involving tip-atom relaxation is required for a more definitive conclusion.

Finally, we point out that lateral force arising from atomic interaction is a conservative force in origin which would yield an average of zero friction if there were no other energy dissipation mechanisms involved. A complete theoretical treatment relating the conservative lateral force to true frictional force has not been available. In most of the theoretical calculations of friction[43-44], it was *simply assumed* that the energy that is required for a tip to move across a potential barrier is subsequently (completely) dissipated into heat. Clearly, additional in depth studies are required to understand this subject.

IV. CONCLUSIONS

The mechanism for microscale variation of friction has been studied. We have shown that local variations in friction generally follow local slope of sample surface. Ratchet mechanism is operative in this scale. We have also developed an analysis to calculate the interatomic forces between atoms of the AFM/FFM tip and those of the sample surface using Fourier expansion of the interatomic potential. We have found that atomic scale friction is related to these forces. Maxima of normal force and those of lateral force do not occur at the same location, thus there is a shift between the peaks in the friction and topography. We also point out that lateral force may play an important role in topographical imaging of graphite surface.

V. ACKNOWLEDGMENT

This research was sponsored by the Office of the Chief of Naval Research, Department of the Navy (Contract No. N00014-93-1-0067). The Contents of the information does not necessarily reflect the position or the policy of the Government and no official endorsement should be inferred.

References

[1] F. P. Bowden and D. Tabor, The Friction and Lubrication of Solids, Clarendon Press, Oxford (1950).

[2] B. Bhushan, Tribology and Mechanics of Magnetic Storage Devices, Springer-Verlag, New York (1990).

[3] G. Binnig, C. F. Quate, and Ch. Gerber, "Atomic Force Microscope", *Phys. Rev. Lett.*, Vol. 56(9), 930-933 (1986).

[4] C. M. Mate, G. M. McClelland, R. Erlandsson, and S. Chiang, "Atomic-Scale Friction of a Tungsten Tip on a Graphite Surface", *Phys. Rev. Lett.*, Vol. 59(17), 1942-1945 (1987).

[5] G. Neubauer, S. R. Cohen, G. M. McClelland, D. Horne, and C. M. Mate, "Force Microscopy with a Bidirectional Capacitance Sensor", *Rev. Sci. Instrum.*, Vol. 61 (9), 2296-2308 (1990).

[6] G. Meyer and N. M. Amer, "Simultaneous Measurement of Lateral and Normal Forces with an Optical-Beam-Deflection Atomic Force Microscope", *Appl. Phys. Lett.*, Vol. 57(20), 2089-2091 (1990).

[7] O. Marti, J. Colchero and J. Mlynek, *Nanotechnology*, Vol. 1, 141 (1990).

[8] C. M. Mate, "Atomic-Force-Microscope Study of Polymer Lubricants on Silicon Surfaces", *Phys. Rev Lett.*, Vol. 68 (22), 3323- 3326 (1992).

[9] R. Erlandsson, G. Hadziioannou, C. M. Mate, G. M. McClelland, and S. Chiang, "Atomic Scale Friction between the Muscovite Mica Cleavage Plane and a Tungsten Tip", *J. Chem. Phys.*, Vol. 89(8), 5190-5193 (1988).

[10] G. J. Germann, S. R. Cohen, G. Neubauer, G. M. McClelland, H. Seki, and D. Coulman, "Atomic Scale Friction of a Diamond Tip on Diamond (100) and (111) surfaces", *J. Appl. Phys.* Vol. 73(1), 163-167 (1993).

[11] M. Hirano, K. Shinjo, R. Kaneko, and Y. Murata, "Anisotropy of Frictional Forces in Muscovite Mica", *Phys. Rev. Lett.*, Vol. 67(19), 2642-2645 (1991).

[12] R. M. Overney, E. Meyer, J. Frommer, D. Brodbeck, R. Lüthi, L. Howald, H. -J. Güntherodt, M. Fujihira, H. Takano, and Y. Gotoh, "Friction Measurements on Phase-Separated Thin Films with a Modified Atomic Force Microscope", *Nature*, Vol. 359, pp. 133-135, 1992.

[13] E. Meyer, R. Overney, D. Brodbeck, L. Howard, R. Lüthi, J. Frommer, and H. -J. Güntherodt, "Friction and Wear of Langmuir-Blodgett Films Observed by Friction Force Microscopy", *Phys. Rev. Lett.*, Vol. 69(12), 1777-1780 (1992).

[14] E. Meyer, R. Overney, R. Lüthi, D. Brodbeck, L. Howald, J. Frommer, H. J. Güntherodt, O. Wolter, M. Fujihira, H. Takano, and Y. Gotoh, "Friction Force Microscopy of Mixed Langmuir-Blodgett Films", *Thin Solid Films,* Vol. 220, 132-137 (1992).

[15] S. J. O'Shea, M. E. Welland, and T. Rayment, "Atomic Force Microscope Study of Boundary Layer Lubrication", *Appl. Phys. Lett.*, Vol. 61(18), 2240-2242 (1992).

[16] J. Ruan and B. Bhushan, "Atomic-Scale Friction Measurements Using Friction Force Microscopy: Part I - General Principles and New Measurement Techniques", *J. Trib., Trans. ASME* (1993).

[17] K. R. Makinson, "On the Cause of the Frictional Difference of the Wool Fiber", *Trans. Faraday Soc.,* Vol. 44, 279-282 (1948).

[18] D. Tabor, "Adhesion and Friction" in The Properties of Diamond (Field, J. E., editor), Academic, New York, pp. 325-350 (1979).

[19] H. A. Mizes, S. Park, and W. A. Harrison, "Multiple-tip Interaction of Anomalous Scanning Tunneling-Microscopy Images of Layered Materials", *Phys. Rev. B* , Vol. 36(8), 4491-4494 (1987).

[20] G. Binnig, Ch. Gerber, E. Stoll, T. R. Albrecht and C. F. Quate, "Atomic Resolution with Atomic Force Microscope", *Europhys. Lett.*, Vol. 3 (12), 1281-1286 (1987).

[21] S. Park and C. F. Quate, "Tunneling Microscopy of Graphite in Air", *Appl. Phys. Lett.*, Vol. 48 (2), 112-114 (1986)

[22] G. Binnig, H. Fuchs, Ch. Gerber, H. Rohrer, E. Stoll, and E. Tosatti, "Energy-Dependent State-Density Corrugation of a Graphite Surface as Seen by Scanning Tunneling Microscopy", *Europhys. Lett.*, Vol. 1 (1), 31-36 (1986).

[23] H. J. Mamin, E. Granz, D. W. Abraham, R. E. Thomson, and J. Clark, "Contamination-Mediated Deformation of Graphite by the Scanning Tunneling Microscope", *Phys. Rev. B*, Vol. 34(2), 9015-9018 (1986).

[24] D. Tomanek, S. G. Loiue, H. J. Mamin, D. W. Abraham, R. E. Thomson, E. Granz, and J. Clarke, "Theory and Observation of highly asymmetric Atomic Structure in Scanning-Tunneling-Microscopy Images of Graphite", *Phys. Rev. B.*, Vol. 35(14), 7790-7793 (1987).

[25] T. R. Albrecht, and C. F. Quate, "Atomic Resolution Imaging of a Nonconductor by Atomic Force Microscopy", *J. Appl. Phys.*, Vol. 62 (7), 2599-2602 (1987).

[26] O. Marti, B. Drake, and P. K. Hansma, "Atomic Force Microscopy of Liquid-Covered Surfaces: Atomic Resolution Images", *Appl. Phys. Lett.*, Vol. 51 (7), 484-486 (1987).

[27] S. A. C. Gould, K. Burke, and P. K. Hansma, "Simple Theory for the Atomic-Force Microscope with a Comparison of Theoretical and Experimental Images of Graphite", *Phys. Rev. B.*, Vol. 40(8), 5363-5366 (1989).

[28] J. M. Soler, A. M. Baro, N. Garcia, and H. Rohrer, "Interatomic Forces in Scanning Tunneling Microscopy: Giant Corrugations of the Graphite Surface", *Phys. Rev. Lett.*, Vol. 57(4), 444-447 (1986).

[29] J. B. Pethica, "Comments on Interatomic Forces in Scanning Tunneling Microscopy: Giant Corrugations in Graphite Surface'", *Phys. Rev. B*, Vol. 57(25), 3235 (1986).

[30] I. P. Batra, N. Garcîa, H. Rohrer, H. Salemink, E. Stoll, and S. Ciraci, "A Study of Graphite Surface with STM and Electronic Structure Calculations", *Surface Science*, Vol. 181, 126-138 (1987).

[31] D. Tomanek, S. G. Louie, "First-Principles calculation of highly asymmetric Structure in Scanning-Tunneling-Microscopy Images of Graphite", *Phys. Rev. B*, Vol. 37(14), 8327-8336 (1988).

[32] J. D. Todd, and J. B. Pethica, "A Shear Model for STM Images of Layered Materials", *J. Phys.: Condensed Matter*, Vol. 1, 9823-9831 (1989).

[33] I. P. Batra and S. Ciraci, "Theoretical Scanning Tunneling Microscopy and Atomic Force Microscopy Study of Graphite Including Tip-Surface Interaction", *J. Vac. Sci. Technol. A* Vol. 6(2), 313-318 (1988).

[34] F. F. Abraham and I. P. Batra, "Theoretical Interpretation of Atomic-Force Microscope Images of Graphite", *Surface Science,* Vol. 209, L125-L132 (1989).

[35] D. Tomanek, G. Overney, H. Miyazaki, S. D. Mahanti, and H. J. Güntherodt, "Theory for the Atomic Force Microscopy of Deformable Surface", *Phys. Rev. B.*, Vol. 63(8), 876-879 (1989).

[36] W. Zhong, G. Overney, and D. Tomanek, "Limits of Resolution in Atomic Force Microscopy Images of Graphite", *Europhys. Lett.*, Vol. 15(1), 49-54 (1991).

[37] G. Overney, D. Tomanek, W. Zhong, Z. Sun, H. Miyazaki, S. D. Mahanti, and H. J. Güntherodt, "Theory for the Atomic Force Microscopy of Layered Elastic Surfaces", *J. Phys.: Condensed Matter*, Vol. 4, 4233-4249 (1992).

[38] T. A. Land, T. Michely, R. J. Behm, J. C. Hemminger, and G. Comsa, "STM Investigation of Single Layer Graphite Structures Produced on Pt(111) by Hydrocarbon Decomposition", Surface Science, Vol. 264, 261-270 (1992).

[39] W. A. Steele, "The Physical Interaction of Gases with Crystalline Solids", *Surf. Sci.*, Vol. 36, 317-352 (1973).

[40] N. W. Ashcroft and N. D. Mermin, Solid State Physics, Holt, Rinehart and Winston, New York, pp. 762-764 (1976).

[41] National Bureau of Standards, Handbook of Mathematical Functions with Formulas, Graphs and Mathematical Tables, John Wiley & Sons, New York (1972).

[42] D. J. Smith, "Atomic Imaging of Surfaces by Electron Microscopy", *Surface Science*, Vol. 178, 462-474 (1986).

[43] W. Zhong, and D. Tomanek, "First-Principles Theory of Atomic-Scale Friction", *Phys. Rev. Lett.*, Vol. 64(25) 3054-7 (1990).

[44] M. Hirano and K. Shinjo, "Atomistic Locking and Friction", *Phys. Rev. B*, Vol. 41(17), 11837-11851 (1990).

Table 1 Location of extremes of force components. The result is for the region where $\frac{dD(2\pi/a,z)}{dz} < 0$ and $D(2\pi/a, z) > 0$ [a is the lattice constant on (0001) graphite plane and is also the distance between the centers of nearest hexagons formed of carbon atoms as shown in Figs. 7 and 9].

	F_x	F_y	F_z
Maximum	$(1/4a, \frac{\sqrt{3}}{2}a)$	(0, 1.474a)	$(0, \frac{a}{\sqrt{3}})$, $(0, \frac{2a}{\sqrt{3}})$
Minimum	$(-1/4a, \frac{\sqrt{3}}{2}a)$	(0, 0.258a)	(0, 0)

Figure captions

1. Schematic of atomic force microscope/friction force microscope (AFM/FFM) using laser beam deflection method.

2 Gray-scale plot of surface profile (σ=5.5 nm), slope of the surface profile (slope profile) taken along the sample sliding direction (mean = -0.09, σ=0.30), and friction profile (mean=1 nN σ=2.5 nN) of a 200 nm x 200 nm scan of a scratched HOPG for a normal load of 42 nN. Light color represents high points in topography, slope and friction profiles and dark points represent corresponding low values. The friction and the slope profiles resemble each other.

3. Gray-scale plot of surface profile (σ=2.4 nm), slope profile (mean = 0, σ=0.175) and friction profile (mean= 1nN, σ=1.7 nN) of a 50 nm x 50 nm scan of a scratched HOPG for a normal load of 42 nN, showing the similarity between the friction and slope profiles.

4. Gray-scale plot of surface profile (σ=5.5 nm), slope profile (mean = -0.006, σ=0.204) and friction profile (mean=2.5 nN, σ=1.7 nN) of a 200 nm x 200 nm scan of a polished single-crystal (IIa) natural diamond for a normal load of 50 nN, showing the similarity between the friction and slope profiles.

5. (a) Gray scale plot of surface topography and friction profile of a 1 nm x 1 nm area of a freshly cleaved HOPG showing the atomic-scale variation of topography and friction. Higher points are shown by lighter color. (b) Schematic of topography and friction profiles shown in (a). The oblate triangles and circles correspond to maxima of topography and friction, respectively. There is a spatial shift between the two.

6. Schematic showing the effect of an asperity shape on local variation in friction in microscale measurements.

7. (a) Hexagonal crystal structure of the (0001) graphite surface showing three staggered layers. (b) Top view of two staggered layers (honeycomb net) shown by the solid (top layer) and dotted (second layer) lines. There are two distinct types of carbon sites in graphite: A-type and B-type. A-type atoms have neighbor atoms directly above and below (solid circles) in the adjacent layers and B-type atoms (open circles) do not have such neighbors. Points "H" on the surface are "hollow" points. Based on analysis presented by Batra et al[33]. and Tomanek et al.[31], B-sites atoms are more prominent than A-sites atoms, thus B-sites atoms are generally observed in STM/AFM imaging (connected by heavy broken lines).

8. A typical STM image of HOPG. Only every other carbon atoms in the surface are "visible" (bright spots) to STM tips, the other half atoms are "missing". Similar results are obtained for AFM (see Fig. 5a).

9. Schematic showing the orientation of the x and y axes relative to the surface structure of graphite. Solid lines connecting to the four open circles form one of several possible choices of a two-dimentional primitive unit cell. The selected location of 2-D unit cell simplifies the calculation. Carbon atoms are located at the vertex of hexagons. Also shown are locations of extremes of normal and lateral forces between a graphite surface and a single (FFM) tip-atom as well as force variation along x and y axes based on a theoretical calculation.

10. Schematics of predicted locations of maxima in normal force (topography) (oblate triangle) and lateral force (circles), assuming that due to lateral force, only every other carbon atom is seen in the normal force profile (topography).

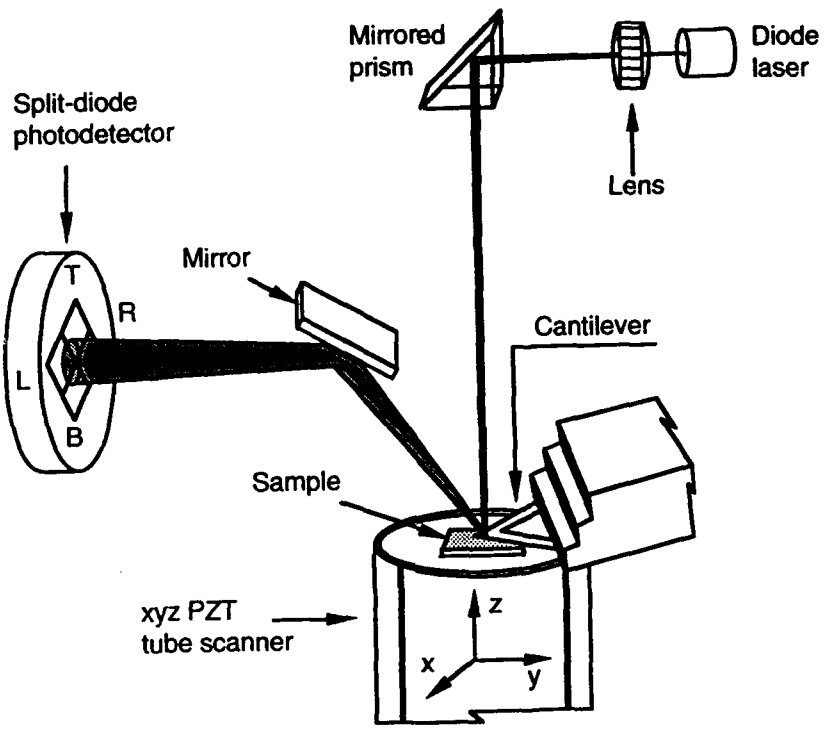
Mirrored
prism
Diode
laser
Split-diode
photodetector
Lens
Mirror
T
R
L
B
Cantilever
Sample
xyz PZT
tube scanner
z
x
y

Fig. 1

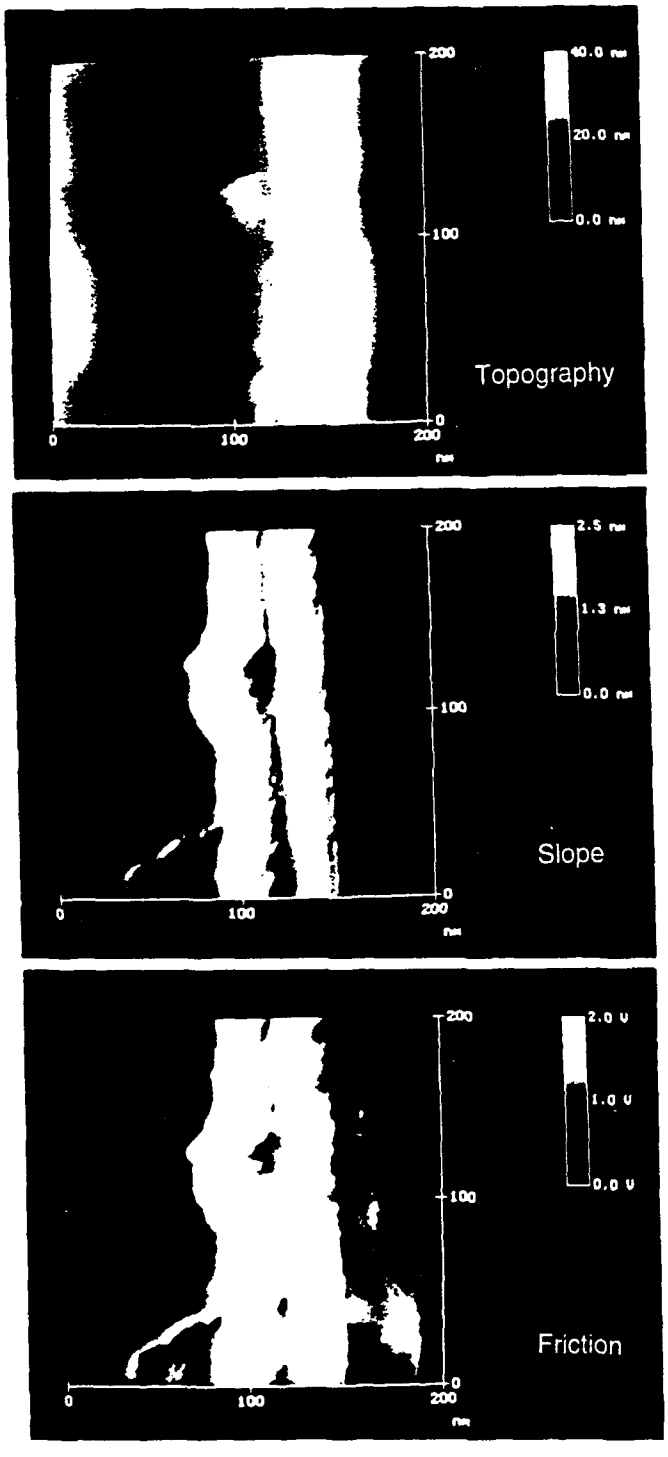
200
100
0
0
100
200
nm
40.0 nm
20.0 nm
0.0 nm
Topography
200
100
0
0
100
200
nm
2.5 nm
1.3 nm
0.0 nm
Slope
200
100
0
0
100
200
nm
2.0 V
1.0 V
0.0 V
Friction

Fig 2

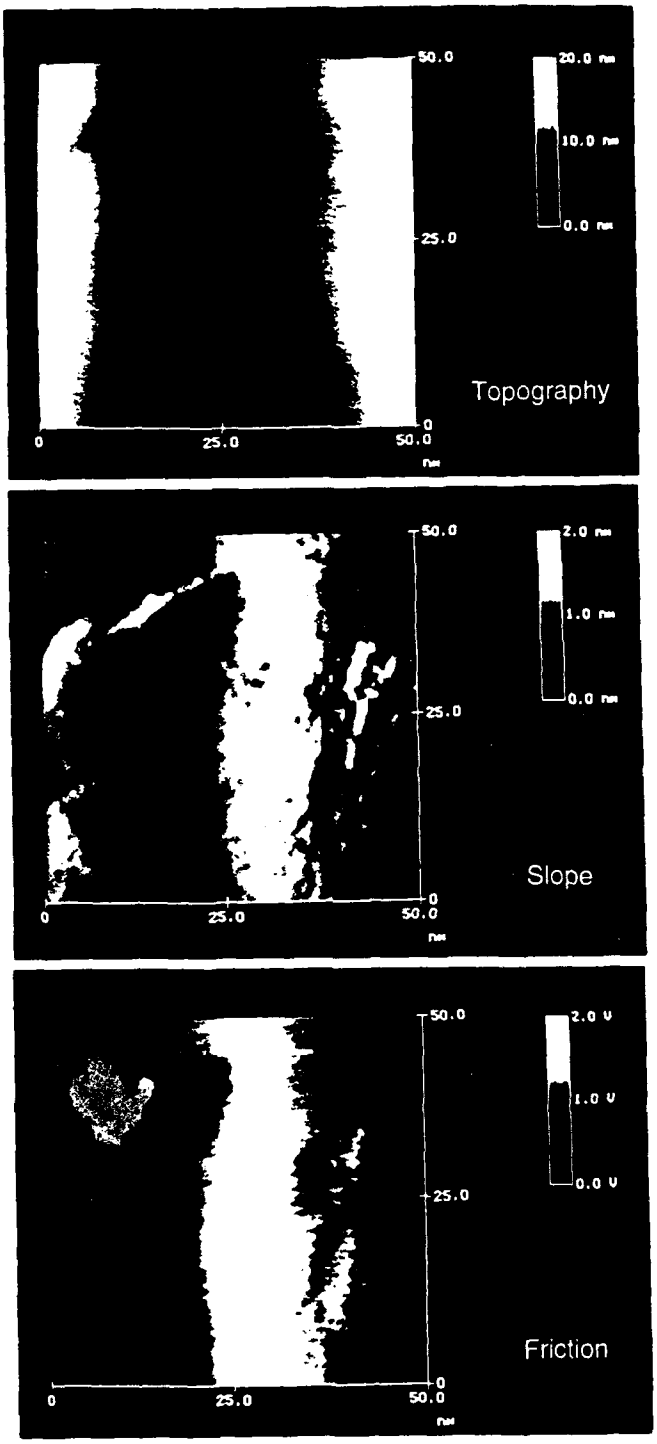
50.0
25.0
0
0
25.0
50.0
nm
20.0 nm
10.0 nm
0.0 nm
Topography
50.0
25.0
0
0
25.0
50.0
nm
2.0 nm
1.0 nm
0.0 nm
Slope
50.0
25.0
0
0
25.0
50.0
nm
2.0 V
1.0 V
0.0 V
Friction

Fig 5

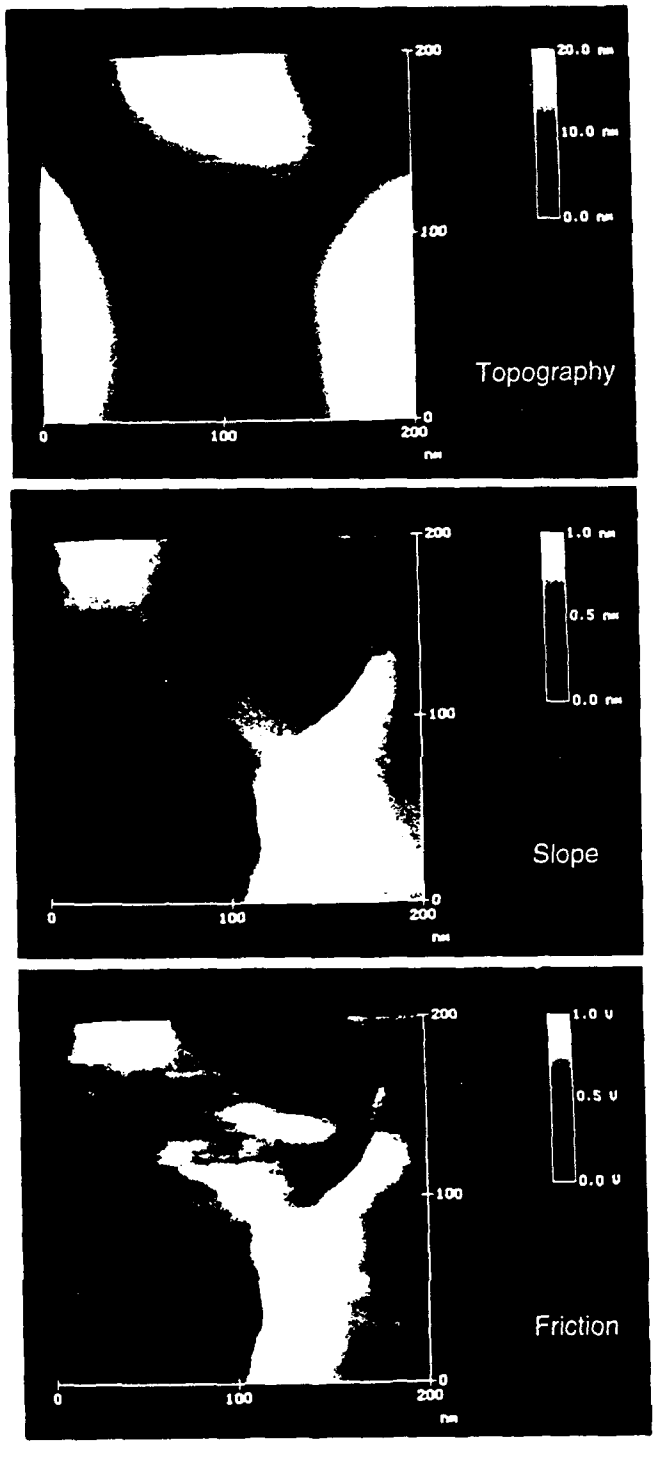
200
100
0
0
100
200
nm
20.0 nm
10.0 nm
0.0 nm
Topography
200
100
0
0
100
200
nm
1.0 nm
0.5 nm
0.0 nm
Slope
200
100
0
0
100
200
nm
1.0 V
0.5 V
0.0 V
Friction

F·24

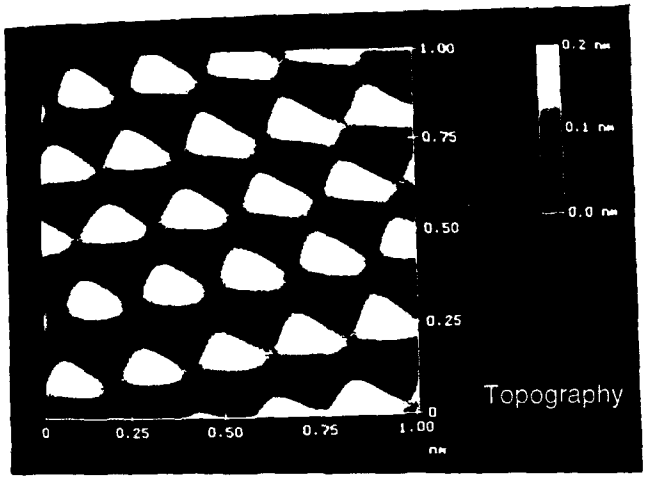
1.00
0.75
0.50
0.25
0
0.25
0.50
0.75
1.00
nm
0.2 nm
0.1 nm
0.0 nm
Topography

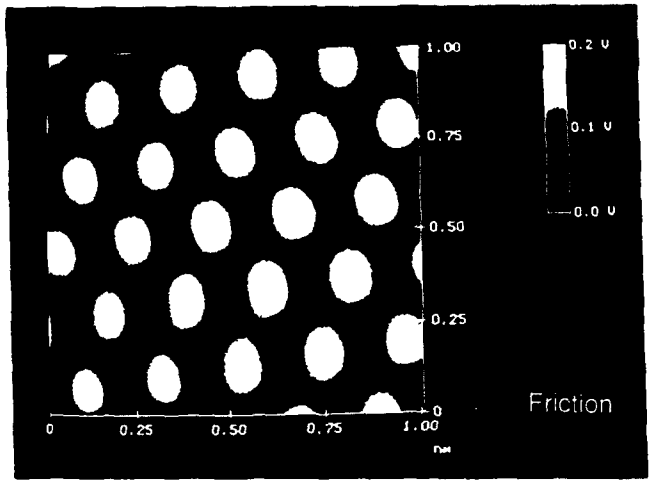
1.00
0.75
0.50
0.25
0
0.25
0.50
0.75
1.00
nm
0.2 V
0.1 V
0.0 V
Friction

Fig 5

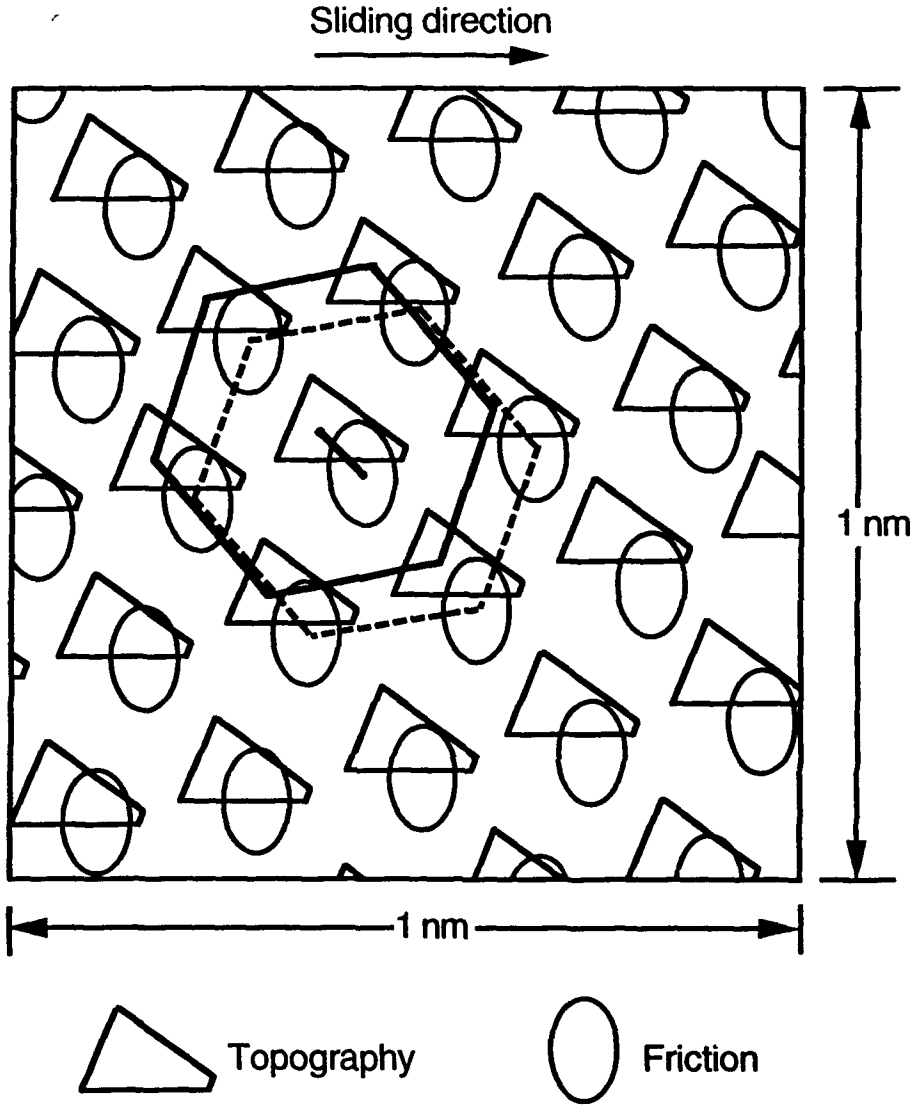

Fig. 5b

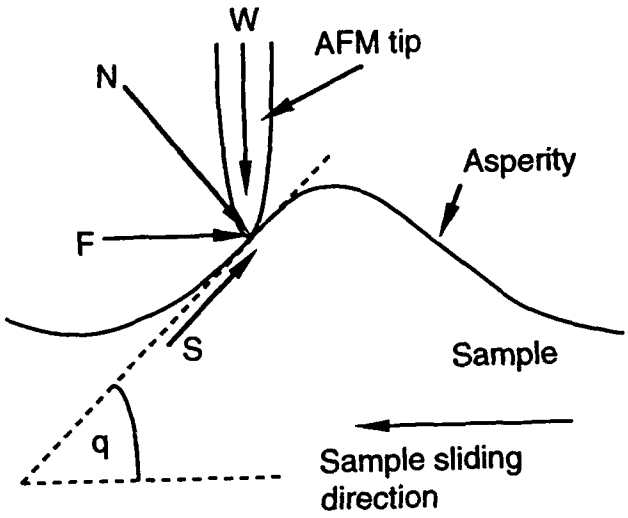

Fig. 6

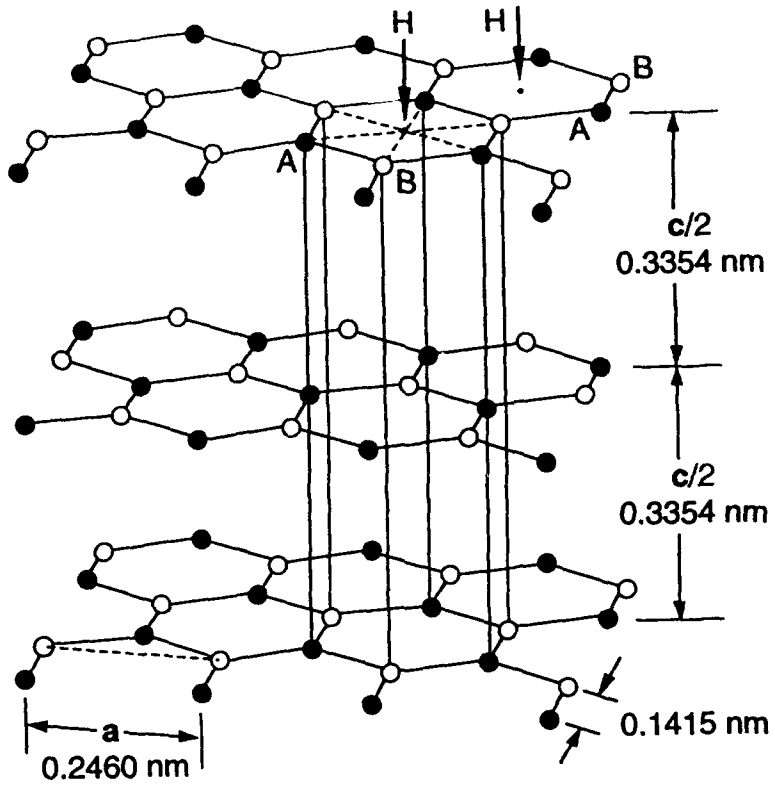
H
H
B
A
A
B
c/2
0.3354 nm
c/2
0.3354 nm
0.1415 nm
a
0.2460 nm

(a)

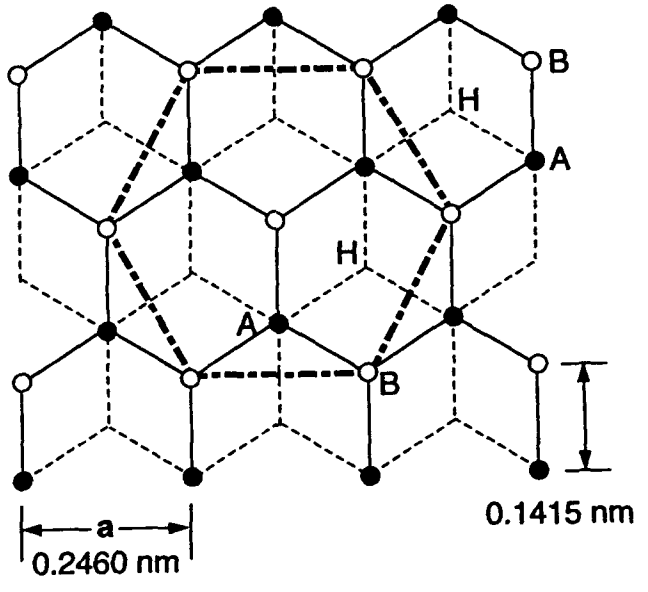
B
H
A
H
A
B
0.1415 nm
a
0.2460 nm

(b)

Fig.7

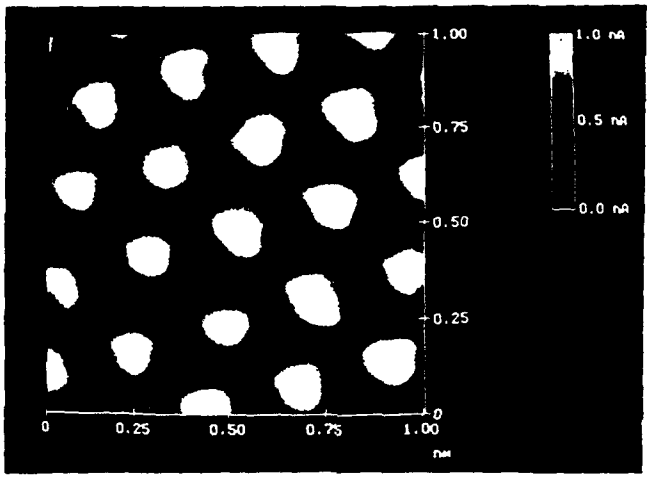

Fig. 8

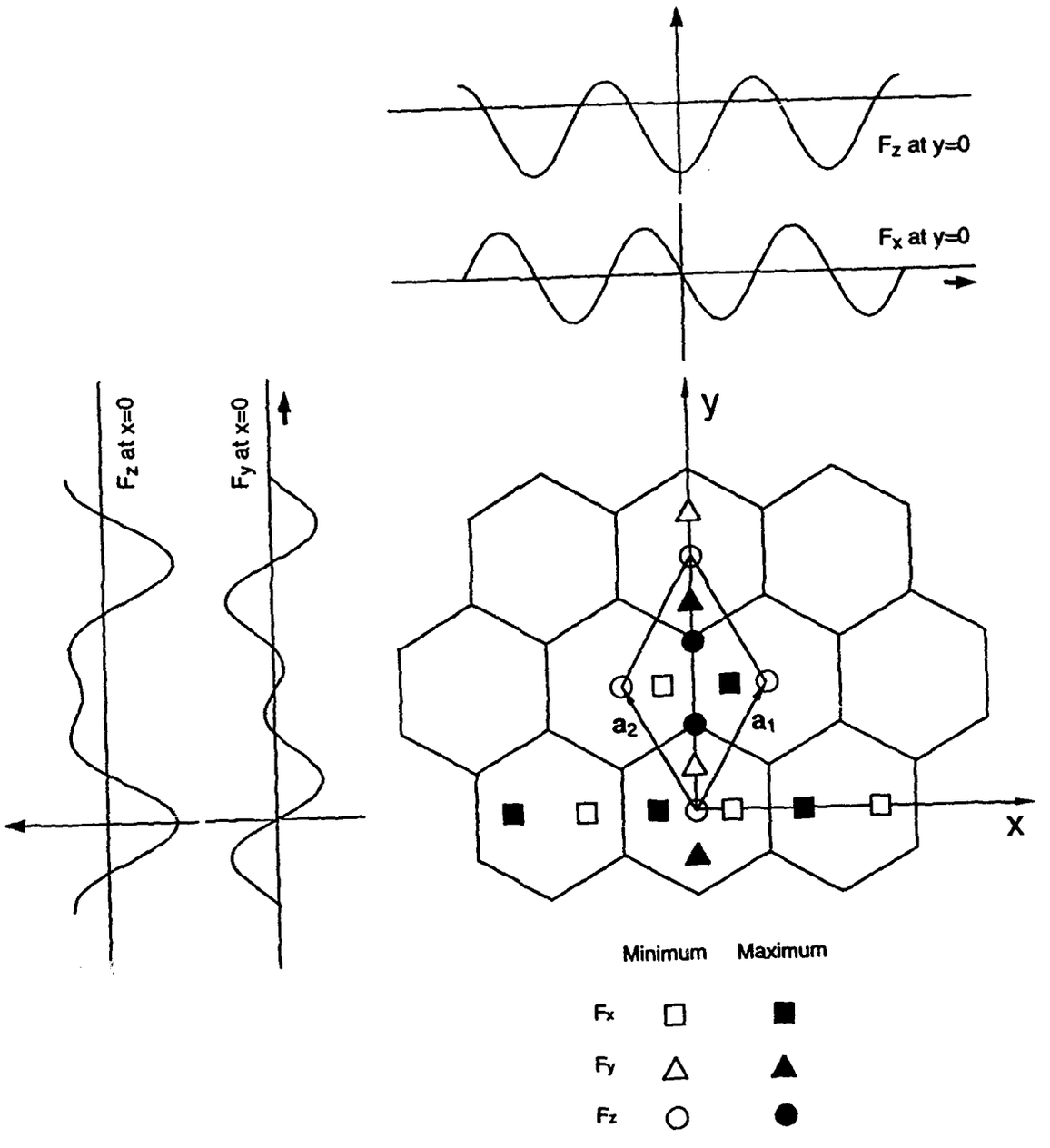
F_z at y=0
F_x at y=0
F_z at x=0
F_y at x=0
y
x
a_2
a_1
Minimum
Maximum
Fx
Fy
Fz

Fig. 9

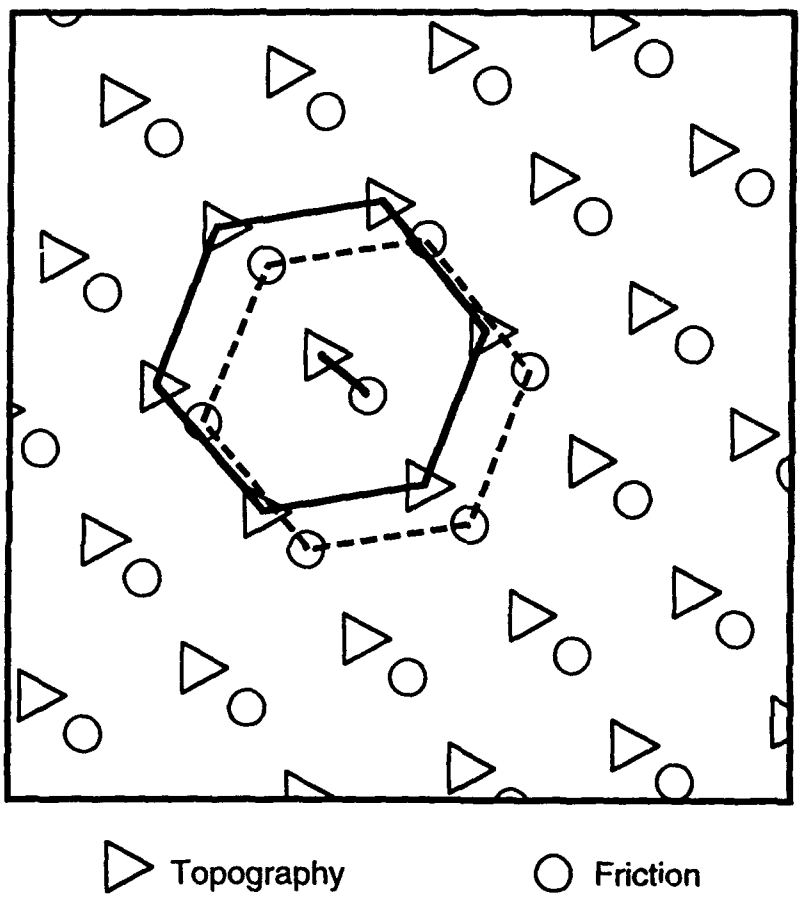

Fig. 10